Cancer Research

Activation of Hematopoietic Stem/Progenitor Cells Promotes Immunosuppression Within the Pre–metastatic Niche

Amber Jin Giles[1], Caitlin Marie Reid[1], Justin DeWayne Evans[1], Meera Murgai[1], Yorleny Vicioso[1], Steven Lorenz Highfill[1], Miki Kasai[1], Linda Vahdat[2], Crystal Lee Mackall[1], David Lyden[3], Leonard Wexler[4], and Rosandra Natasha Kaplan[1]

Abstract

Metastatic tumors have been shown to establish microenvironments in distant tissues that are permissive to disseminated tumor cells. Hematopoietic cells contribute to this microenvironment, yet the precise initiating events responsible for establishing the pre-metastatic niche remain unclear. Here, we tracked the developmental fate of hematopoietic stem and progenitor cells (HSPC) in tumor-bearing mice. We show that a distant primary tumor drives the expansion of HSPCs within the bone marrow and their mobilization to the bloodstream. Treatment of purified HSPCs cultured *ex vivo* with tumor-conditioned media induced their proliferation as well as their differentiation into immunosuppressive myeloid cells. We furthered tracked purified HSPCs *in vivo* and found they differentiated into myeloid-derived suppressor cells in early metastatic sites of tumor-bearing mice. The number of $CD11b^{+}Ly6g^{+}$ cells in metastatic sites was significantly increased by HSPC mobilization and decreased if tumor-mediated mobilization was inhibited. Moreover, pharmacologic mobilization of HSPCs increased metastasis, whereas depletion of $Gr1^{+}$ cells abrogated the metastasis-promoting effects of HSPC mobilization. Finally, we detected elevated levels of HSPCs in the circulation of newly diagnosed cancer patients, which correlated with increased risk for metastatic progression. Taken together, our results highlight bone marrow activation as one of the earliest steps of the metastatic process and identify circulating HSPCs as potential clinical indicators of metastatic niche formation. *Cancer Res; 76(6); 1335–47. ©2015 AACR.*

Introduction

Metastasis remains the most lethal aspect of cancer, yet identifying patients with systemic disease who will develop metastatic progression remains a challenge (1). Successful metastatic progression from disseminating tumor cells likely involves a combination of tumor-intrinsic characteristics and extrinsic signals from the local milieu of the distant site, much like stem cells within their specialized microenvironment, or niche (2–4). Microenvironmental signals impact disseminating tumor cells and regulate quiescence or proliferation, survival or apoptosis, and renewal or differentiation (5–7). The cell fate decision of these seeding tumor cells dictates metastatic progression and ultimately drives clinical outcome.

Previously, we demonstrated that tumor-derived factors form a metastasis-conducive microenvironment by activating resident stromal cells and recruiting bone marrow–derived $VEGFR1^{+}$ progenitor cells (8). This process, which we termed the "premetastatic niche," not only introduced nonneoplastic cells as key players in metastatic progression, but also conveyed that cancer is systemic, utilizing niche biology for its dispersion (9, 10). Others have confirmed and expanded the concept of the premetastatic niche, enforcing its essential role in the metastatic process (10–20). However, the initiating events that lead to premetastatic niche formation remain unclear. Moreover, a marker for premetastatic niche initiation in patients could provide a useful new addition to current approaches to stratify patients based on metastatic risk.

Our data suggest mobilized hematopoietic stem and progenitor cells (HSPC) emerging from tumor-mediated activation of the bone marrow can be used to monitor the metastatic process. HSPC production and mobilization are elevated in cancer patients and murine models before detectable metastases and foster an immunosuppressive milieu within the premetastatic niche of distant tissue sites. This is the first study to directly track the developmental fate of HSPCs in tumor-bearing hosts to identify the origins of myeloid-derived suppressor cell (MDSC) formation. HSPCs represent a powerful tool as a potential novel approach to direct therapies based upon reestablishing the balance of altered hematopoiesis.

Materials and Methods

Mice

C57BL/6, CD45.1, cBrd, and Scid/Beige mice were obtained from the Animal Production Program, NCI (NCI, Frederick, MD). GFP transgenic mice [C57BL/6-Tg(UBC-GFP)30Scha/J] were

[1]Pediatric Oncology Branch, NCI, NIH, Bethesda, Maryland. [2]Department of Medicine, Division of Hematology and Oncology, Weill Cornell Medical College, New York, New York. [3]Children's Cancer and Blood Foundation Laboratories, Departments of Pediatrics, Cell and Developmental Biology, Weill Cornell Medical College, New York, New York. [4]Department of Pediatrics, Memorial Sloan Kettering Cancer Center, New York, New York.

Note: Supplementary data for this article are available at Cancer Research Online (http://cancerres.aacrjournals.org/).

Corresponding Author: Rosandra Natasha Kaplan, NCI Center for Cancer Research, NIH, 10 Center Drive MSC 1100, Bethesda, MD 20892. Phone: 301-496-1735; Fax: 301-451-7052; E-mail: kaplanrn@mail.nih.gov

doi: 10.1158/0008-5472.CAN-15-0204

purchased from Jackson Laboratories. Mice were bred and maintained under specific pathogen-free conditions at the NIH animal facility. All studies were performed according to protocols approved by the NCI Animal Care and Use Committee.

Bone marrow transplants

C57BL/6 mice were lethally irradiated (950 cGy) with a cesium irradiator on day 0 and transplanted with 5×10^6 total bone marrow cells from GFP transgenic mice on day 1. A hematopoietic reconstitution period of 4 weeks passed before chimeric mice were used for experiments.

Tumor injection

For orthotopic tumor inoculations, cells were prepared as single-cell suspensions after trypsin digestion and injected into the mammary fat pad (E0771) or gastrocnemius muscle (M3-9-M) in 50-μL Hank's Balanced Salt Solution (HBSS) using a sterile 27.5 gauge needle. Mice were humanely euthanized when tumor size reached 20 mm in any direction. For experimental metastasis studies, single-cell suspensions of tumor were injected by tail vein in 0.1-mL HBSS using a 27.5 gauge needle.

AMD3100 (Sigma) was administered by intraperitoneal injection (125 μg/mouse) in 0.1-mL PBS using a 27.5 gauge needle. AC-220 was dissolved in 22% hydroxypropyl β cyclodextrin (CTD) and administered daily by oral gavage. AC-220 dosage was 5 mg/kg/day.

Bioluminescence

Anesthetized mice received intraperitoneal injection of 3 mg D-luciferin (Promega). Display and image analyses were performed using Living Image software (Xenogen Corporation).

T-cell immunosuppression assay

Untouched splenic T cells were isolated from C57BL/6 spleens using a T-cell Negative Depletion Kit (Miltenyi Biotec) and stained with 5 μmol/L CellTrace Violet. T cells were stimulated with anti-CD3/CD28 Dynabeads (Gibco) at a 2:1 ratio of T cells:beads. Assay was performed in RPMI1640 containing physiologic levels of L-arginine (150 μmol/L) supplemented with 10% fetal calf serum, 50 μmol/L 2-mercaptoethanol, 10 mmol/L N-2-hydroxyethylpiperazine-N′-2-ethane sulfonic acid buffer, 1 mmol/L sodium pyruvate, and 100 U/mL penicillin/streptomycin. N^W-hydroxy-nor-arginine (Nor-NOHA) and L-N^G-monomethyl-arginine-citrate (L-NMMA) were each used at 300 μmol/L.

Humans

Normal human peripheral blood samples were obtained with informed consent from healthy children 1 to 25 years of age and healthy adults who were hepatitis A, B, C, and HIV negative by serology obtained with informed consent at Weill Cornell Medical Center (New York, NY) according to an IRB-approved protocol (WMC IRB 0604008488). Peripheral blood cells were obtained with informed consent from previously untreated patients at Memorial Sloan Kettering Cancer Center and Weill Cornell Medical Center according to IRB-approved protocols (MSKCC IRB 03-099 and WMC IRB 0604008488). To protect patient privacy, samples were decoded according to approved IRB procedures, whereas relevant clinical information was made available to the researchers upon request.

Colony forming assays

For mouse colony forming units (CFU), red blood cell–lysed peripheral blood and bone marrow of control or tumor-bearing mice were seeded in triplicate at 100,000 cells/well into 6-well culture plates with M3434 methylcellulose (Stem Cell Technologies). Plates were imaged 12 days later with a Zeiss microscope and scored.

For human CFU, unseparated peripheral blood mononuclear cells (PBMC; 2×10^5) were cultured in triplicate in methylcellulose (MethoCult H4034 Optimum) containing 2% fetal calf serum (FCS) and Iscove's Modified Dulbecco's Medium according to the manufacturer's technical resource manual. Plates were incubated at 37°C in 5% CO_2 and full humidity. After a culture period of 14 days, cultures were examined under an inverted microscope. Aggregates with at least 50 translucent, compact, or dispersed cells were counted as CFU-GM. The mean colony numbers ± SEM are shown.

Cell lines

E0771 tumor cell line was grown in RPMI1640 with 10% FCS and 1% penicillin/streptomycin. M3-9-M tumor cell line was grown in RPMI1640 with 10% FCS, 1% penicillin/streptomycin, 1% HEPES buffer, 1% nonessential amino acids, 1% sodium pyruvate, 1% L-glutamine, and 50 μmol/L 2-mercaptoethanol. Mesenchymal stem cells (Gibco) were grown in DMEM/F-12 medium with GlutaMAX-I, 10% MSC-qualified FCS, and 1% penicillin/streptomycin. Mesenchymal stem cells were discarded after passage 10.

RayBio cytokine array

E0771 and M3-9-M were grown in RPMI1640 with 1% FCS and 1% penicillin/streptomycin overnight. Tumor-conditioned media were centrifuged and passed through a 0.22-μm filter prior to use in the array. RayBio C1000 array was used to detect tumor-secreted cytokines.

Ex vivo bone marrow culture

Lineage-depleted bone marrow was collected using the EasySep mouse hematopoietic progenitor cell enrichment kit. Cells were cultured for 7 days in StemSpan serum-free expansion medium with 25 ng/mL recombinant murine FLT3 ligand and 1× antibiotic–antimycotic (Gibco). Cultures were fed on day 4. Bone marrow LSK cells were cultured for seven days with M3-9-M RMS or E0771 BCA tumor-conditioned medium, control medium with or without the addition of vehicle or FLT3 inhibitor AC-220 (NCI Developmental Therapeutics Program).

Murine tissue collection

Peripheral blood was collected with heparinized glass capillary tubes from retro-orbital sinus of anesthetized mice into EDTA-coated tubes. Bone marrow was collected by flushing femurs with PBS containing 1% FCS and 1 mmol/L EDTA. Lungs were perfused with normal saline to remove peripheral blood and minced with a scalpel. Lung pieces were digested in DMEM with 1 mg/mL type I collagenase at 37°C for 30 minutes with gentle agitation. Lung fragments were dissociated by pressing against a 70-μm nylon filter.

Flow cytometry and sorting

Cells were lineage depleted prior to sorting using an EasySep Lineage Depletion Kit (Stem Cell Technologies). Lineage-negative cells were stained for Lineage, c-Kit, and Sca-1. Live cells were

identified by exclusion of viability dye. Cell sorting was performed on a FACSAria II cell sorter.

For flow cytometry analysis, single-cell suspensions of mouse tissues were prepared from murine tissues and stained in 0.5% BSA/PBS with 0.05% NaN_3. Total cell counts were determined from Trypan exclusion of cell suspensions. Antibodies were purchased from eBiosciences, BioLegend, and Stem Cell Technologies. Flow cytometry data were acquired on a BD LSRFortessa and analyzed with FlowJo software (Tree Star).

For human samples, peripheral blood isolated from either healthy human donors or from newly diagnosed previously untreated patients with rhabdomyosarcoma or breast carcinoma. The mononuclear fractions were extracted following Ficoll-Paque Plus (GE Healthcare Life Sciences) density gradient centrifugation according to standard methods (density, 1.077 g/mL; 400 × *g* for 30 minutes) and analyzed fresh. Mononuclear fraction isolated after Ficoll density gradient centrifugation underwent red blood cell lysis using ACK Lysing Buffer (Life Technologies) using standard protocol. The cells were counted using 3% acetic acid with methylene blue mixed with Trypan blue and stained for flow cytometry analysis after Fc blockade.

Microscopy

Immunofluorescence. Tissues were frozen in OCT compound (Tissue-Tek), and 10-μm serial sections (cryostat, Leica) were used for staining. Sections were fixed in ice-cold methanol. Markers and antibodies were: 4,6′-diamidino-2-phenylindole (DAPI) for DNA, Alexa Fluor 488–conjugated Gr-1, and APC-conjugated anti-Gr-1. Rabbit anti-GFP (Abcam) was detected with donkey anti-rabbit Cy3 (Jackson ImmunoResearch). Images were acquired with an Axio Observer Z1 inverted microscope with a 63× Plan-Apochromat oil objective (Zeiss).

Diff-Quik staining. Cytospin preparations of sorted $CD11b^+Gr\text{-}1^+$ cells were stained with Diff-Quik as per the manufacturer's protocol.

RNA isolation

Femur bones were dissected from HBSS-treated control mice and E0771 tumor-bearing mice at 12 days posttumor injection, and flash-frozen in liquid nitrogen. Whole bone was crushed in TRIzol using a homogenizer at 40-second intervals. Total RNA was isolated and precipitated from TRIzol using chloroform/ethanol extraction, and further purified and DNase I treated using the Qiagen MicroRNA Isolation Kit. RNA concentration and quality was assessed by an Agilent 2100 Bioanalyzer.

Primer sequences

Primer	Sequence
CXCL12-F	TGCATCAGTGACGGTAAACCA
CXCL12-R	TTCTTCAGCCGTGCAACAATC
B-actin-F	GGCTGTATTCCCCTCCATCG
B-actin-R	CCAGTTGGTAACAATGCCATGT

Quantitative real-time PCR

cDNA synthesis was performed on 1 μg RNA per sample using the Bio-Rad iScript cDNA Synthesis Kit and qRT-PCR was performed using the Bio-Rad SsoAdvanced system and iCycler technology.

Statistical analysis

For human studies, statistics were calculated using Prism 4.0 software (GraphPad Software, Inc.). The Welch corrected Student *t* test was used to calculate all column statistics when the data were normal by D'Agostino & Pearson omnibus normality test. If data were nonparametric, a Mann–Whitney test was used. Two-tailed *P* values are shown in figures. For comparison of groups, one-way ANOVA or Kruskal–Wallis test (for nonparametric data) were used. For murine studies, data are presented as averages with SD. Statistical comparisons between groups were performed using unpaired Student *t* tests to calculate the two-tailed *P* value. *P* values <0.05 were considered significant.

Results

Hematopoietic stem cells expand in response to a growing primary tumor

We first defined tumor growth rate and metastatic progression after orthotopic injection for two C57BL/6 syngeneic tumor cell lines: the E0771 breast carcinoma (BCA) and M3-9-M rhabdomyosarcoma cell lines (ERMS; Supplementary Fig. S1). Primary tumors release tumor cells early during tumor development, but the majority of these cells die upon vascular arrest or extravasation into distant tissues (21, 22). To detect low numbers of disseminated luciferase-expressing tumor cells, we utilized the *in vivo* imaging system (IVIS). In both models, we identified a period before overt metastasis when either no cells or single tumor cells were detected in distant tissues. We termed this period "metastatic tumor seeding" and determined that it occurred during the formation of the premetastatic niche.

We investigated the bone marrow as a potential source of the key hematopoietic component of the premetastatic niche and as one of the earliest targets of tumor-secreted factors given its integral role in the stress response to inflammation. The $Lineage^-$ $Sca1^+$ $c\text{-}Kit^+$ (LSK) gate was utilized to identify the total population of HSPCs within the bone marrow (Fig. 1A). Notably, these LSK HSPCs expressed VEGFR1, a potential marker for this population that is consistent with our previous studies (Fig. 1B; ref. 8). The total number of LSK HSPCs in the bone marrow of tumor-bearing E0771 BCA and M3-9-M ERMS mice significantly increased within the 2 weeks following tumor implantation and their numbers doubled, relative to basal levels, during the period of metastatic tumor seeding (Fig. 1C and D). Bromodeoxyuridine (BrdUrd) uptake analysis demonstrated a greater number of proliferating LSK cells in the bone marrow of premetastatic E0771 BCA tumor-bearing mice relative to controls (Fig. 1E). Furthermore, a significantly greater proportion of the LSK population was proliferating in tumor-bearing relative to control mice (40% vs. 19%, respectively; Fig. 1F).

LSK HSPCs can be subdivided by flow cytometric analysis into $Flt3^-CD34^-CD48^-CD150^+$ long-term (LT-HSC), $Flt3^-CD34^+$ short-term (ST-HSCs), and $Flt3^+CD34^+$ multipotent progenitors (MPP). LT-HSCs, which are resistant to cycling and represent the most stem-like population of HSPCs, maintained basal levels until later stages of tumor development (Fig. 1G and J; refs. 23, 24). However, ST-HSCs and MPPs expanded during initiation of the premetastatic niche of both E0771 BCA and M3-9-M ERMS tumor-bearing mice (Fig. 1H, I, K, and L). Together, these data demonstrate hematopoiesis is activated in response to a growing

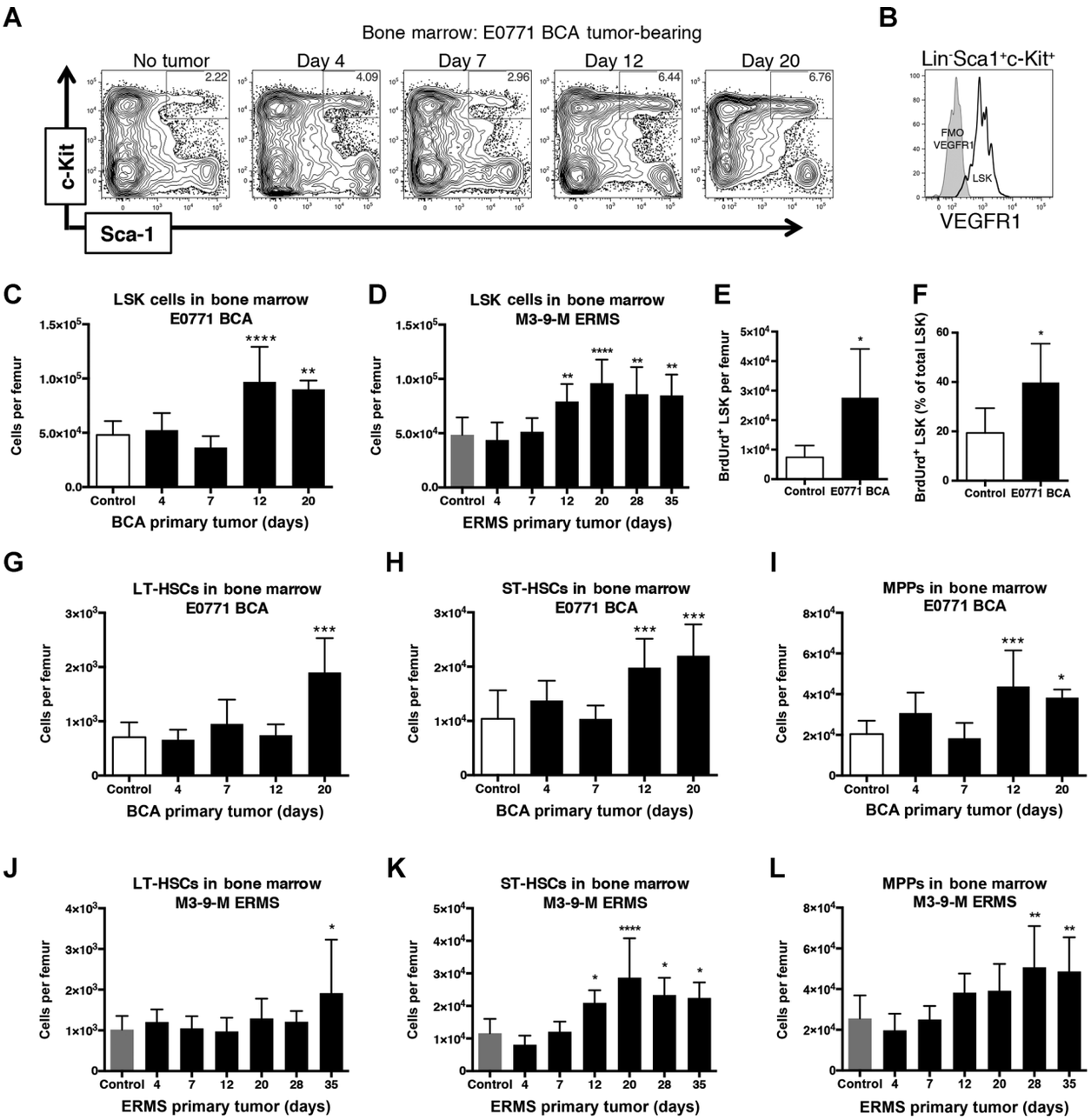

Figure 1.

Primary tumor increases stem cell subsets in bone marrow. A, representative flow cytometry plots of RBC-lysed total bone marrow previously gated to exclude doublets, dead cells, and lineage-positive cells. HBSS control or E0771 BCA tumor-bearing mice at the indicated times postorthotopic injection are shown. B, flow cytometry analysis of VEGFR1 expression on LSK-gated bone marrow. C, quantification of LSK cells per femur of control or E0771 BCA tumor-bearing mice at the indicated times following tumor implantation ($n = 10$ for no tumor mice; $n = 5$–10 for each tumor-bearing mouse group). D, quantification of LSK cells per femur of control or M3-9-M ERMS tumor-bearing mice at the indicated times following tumor implantation ($n = 11$ for no tumor mice; $n = 4$–9 for each tumor-bearing mouse group). E, total number of LSK that had incorporated BrdUrd in control mice or mice-bearing E0771 BCA orthotopic tumors for 12 days ($n = 5$ per group). F, percentage of the LSK population that had incorporated BrdUrd in control or E0771 BCA tumor-bearing mice 12 days following orthotopic tumor implantation ($n = 5$ per group). G–I, quantification of hematopoietic stem cell subsets per femur of control or E0771 BCA tumor-bearing mice at the indicated times following tumor implantation ($n = 10$ for no tumor mice; $n = 5$–10 for each tumor-bearing mouse group). J–L, quantification of hematopoietic subsets per femur of control or M3-9-M ERMS tumor-bearing mice at the indicated times following tumor implantation ($n = 11$ for no tumor mice; $n = 4$–9 for each tumor-bearing mouse group). *, $P < 0.05$; **, $P < 0.005$; ***, $P < 0.005$; ****, $P < 0.0001$.

tumor, resulting in expansion of hematopoietic progenitor populations within the bone marrow.

HSPCs are mobilized during premetastatic niche initiation and contribute to myeloid subsets in premetastatic sites

Flow cytometry analysis of peripheral blood revealed significantly elevated numbers of LSK HSPCs during formation of the premetastatic niche in both the E0771 BCA and M3-9-M ERMS models (Fig. 2A and B). Elevated levels of stem-like hematopoietic progenitor cells in the peripheral blood of premetastatic mice were confirmed functionally with a CFU assay (Fig. 2C). Together, these data demonstrate that LSK HSPCs expand and mobilize in response to a growing primary tumor. Because these events occurred during pre/early metastatic period, we sought to determine whether expanded LSK HSPCs in circulation contributed to hematopoietic cell types within the premetastatic site.

Mobilized stem cells rapidly home to and migrate through peripheral tissues. To track the developmental fate of mobilized LSK HSPCs *in vivo*, LSK HSPCs were sorted from E0771 BCA tumor-bearing CD45.1$^+$ mice and intravenously injected into either E0771 BCA tumor-bearing or control CD45.2$^+$ recipients. CD45.1$^+$ donor cells were detected in lung, tumor, and bone marrow 24 hours after injection, demonstrating that circulating LSK cells can home to multiple tissues (Fig. 2D). Interestingly, 3.4-fold fewer donor cells homed to the bone marrow of tumor-bearing mice. We hypothesized that decreased homing of HSPCs to the bone marrow was linked to increased LSK HSPC mobilization observed in tumor-bearing mice. qPCR analysis revealed that the LSK homing cytokine *Cxcl12* was significantly downregulated in the bones of premetastatic tumor-bearing mice (Supplementary Fig. S2A). Consistent with this, peripheral blood of tumor-bearing mice also contained elevated levels of CXCR4-expressing LSK cells, suggesting that the CXCR4:CXCL12 signaling axis may contribute to stem cell mobilization in tumor-bearing mice (Supplementary Fig. S2B–S2D).

Within the lung of tumor-bearing recipients, twice as many donor-derived LSK HSPCs developed into CD11b$^+$ cells compared with nontumor bearing mice, including significantly greater numbers of CD11b$^+$Ly6g$^+$ and CD11b$^+$Ly6c^{high} cells (Fig. 2E–G). Immunofluorescence of tumor-bearing mice revealed CD11b$^+$ myeloid cells that coexpressed Gr-1, consistent with a phenotype of immunosuppressive MDSCs. These immunosuppressive cells were found in close proximity to GFP-expressing spontaneous tumor metastases in the lungs of E0771 BCA tumor-bearing mice (Fig. 2H and Supplementary Fig. S3A–S3C). MDSCs within a primary tumor possess strong immunosuppressive properties (25–27). Indeed, E0771 BCA tumor-bearing mice developed immunosuppressive MDSCs within the primary tumor and spleen (Supplementary Fig. S4). Thus, we tested the functional capability of CD11b$^+$Gr-1$^+$ cells from premetastatic lungs to suppress anti-CD3/anti-CD28-mediated T-cell proliferation. Tumor-bearing E0771 BCA and M3-9-M ERMS mice displayed elevated numbers of CD11b$^+$Ly6g$^+$ and CD11b$^+$Ly6c^{high} cells and CD11c$^+$ cells in pre/early metastatic lung (Supplementary Fig. S5A–S5F). At these times other myeloid subsets, such as tumor-associated macrophages (CD11b$^+$Ly6c^{high}F4/80$^+$CD115$^+$), M2 macrophages (CD11b$^+$Ly6c^{high}CD206$^+$CD115$^+$), and M1 macrophages (CD11b$^+$Ly6c^{high}CD80$^+$) were not increased relative to control mice (Supplementary Fig. S5GE–S5I). To assess the immunosuppressive function of MDSCs in lung, CD11b$^+$Gr-1$^+$ myeloid cells, which encompassed both granulocytic MDSCs and monocytic MDSCs, were sorted from the lungs of premetastatic tumor-bearing mice. Importantly, these lungs had no evidence of metastasis based on luciferase activity. The majority of sorted Gr-1$^+$ MDSCs had the characteristic ring-shaped morphology of granulocytic MDSCs (Fig. 2I). Sorted CD11b$^+$Gr-1$^+$ myeloid cells from the lungs of E0771 BCA premetastatic mice possessed powerful immunosuppressive capacity and suppressed anti-CD3/anti-CD28-stimulated T-cell proliferation by approximately 50% (Fig. 2J).

MDSCs suppress T-cell activation through several mechanisms, including depletion of L-arginine through arginase-1 or by production of nitric oxide and reactive oxygen species with inducible nitric oxide synthase (iNOS; ref. 28). To determine whether the MDSCs isolated from premetastatic lungs utilized these pathways to mediate T-cell suppression, we performed a T-cell suppression assay in the presence of the arginase inhibitor, NOR-NOHA, or the iNOS inhibitor, L-NMMA. MDSCs cultured with L-NMMA, but not NOR-NOHA, were significantly impaired in their ability to suppress T-cell proliferation (Fig. 2K). Therefore, MDSCs found within premetastatic or early metastatic sites are functionally capable of suppressing T-cell proliferation, and the suppression is mediated in part by iNOS activity.

LSK HSPCs expand in response to tumor-derived factors and differentiate into immunosuppressive myeloid lineages

We next utilized *ex vivo* culture to determine whether the tumor-derived factors directed LSK HSPC expansion or differentiation into immunosuppressive myeloid lineages. Lineage-depleted bone marrow was cultured for 1 week with StemSpan or StemSpan conditioned by E0771 BCA or M3-9-M ERMS, and LSK and myeloid subsets were quantified by flow cytometry. All culture conditions were supplemented with 25 ng/mL FLT3 ligand, an essential cytokine for *ex vivo* HSPC culture. E0771 BCA and M3-9-M ERMS tumor-conditioned media (TCM) significantly expanded LSK HSPCs relative to control medium (57- and 9-fold over StemSpan alone, respectively; Fig. 3A). In addition, CD11b$^+$Ly6g$^+$ and CD11b$^+$Ly6c^{high} subsets were also significantly increased with TCM (Fig. 3B and C).

As both HSPCs and myeloid subsets were expanded with TCM, we sought to determine whether LSK HSPCs directly contributed to myeloid populations. Flow cytometry–sorted LSK cells were cultured with plain medium or E0771 BCA TCM. Once again, myeloid cells were significantly expanded as assessed by CD11b$^+$, CD11b$^+$Ly6g$^+$, and CD11b$^+$Ly6c^{high} staining (Fig. 3D–F). Furthermore, cells derived from LSK cultured with E0771 BCA TCM demonstrated potent, dose-dependent T-cell–suppressive capability (Fig. 3G). Interestingly, cells derived from LSK cultured with control medium significantly promoted T-cell expansion relative to T cells cultured with anti-CD3/anti-CD28 microbeads alone, demonstrating that cells derived from LSK culture are not made immunosuppressive by culture conditions alone.

The potential for TCM to expand LSK diminished rapidly when the media were heated, increasing temperatures prior to culture, leading us to investigate protein factors as mediators of this process (Supplementary Fig. S6A–S6D). Cytokine analysis of E0771 BCA and M3-9-M ERMS TCM identified multiple factors that can contribute to LSK expansion, including FLT3 ligand (Supplementary Table S1). FLT3 ligand is critical for LSK maintenance and synergizes with other cytokines to promote stem cell expansion (29). Consistent with these observations, recombinant

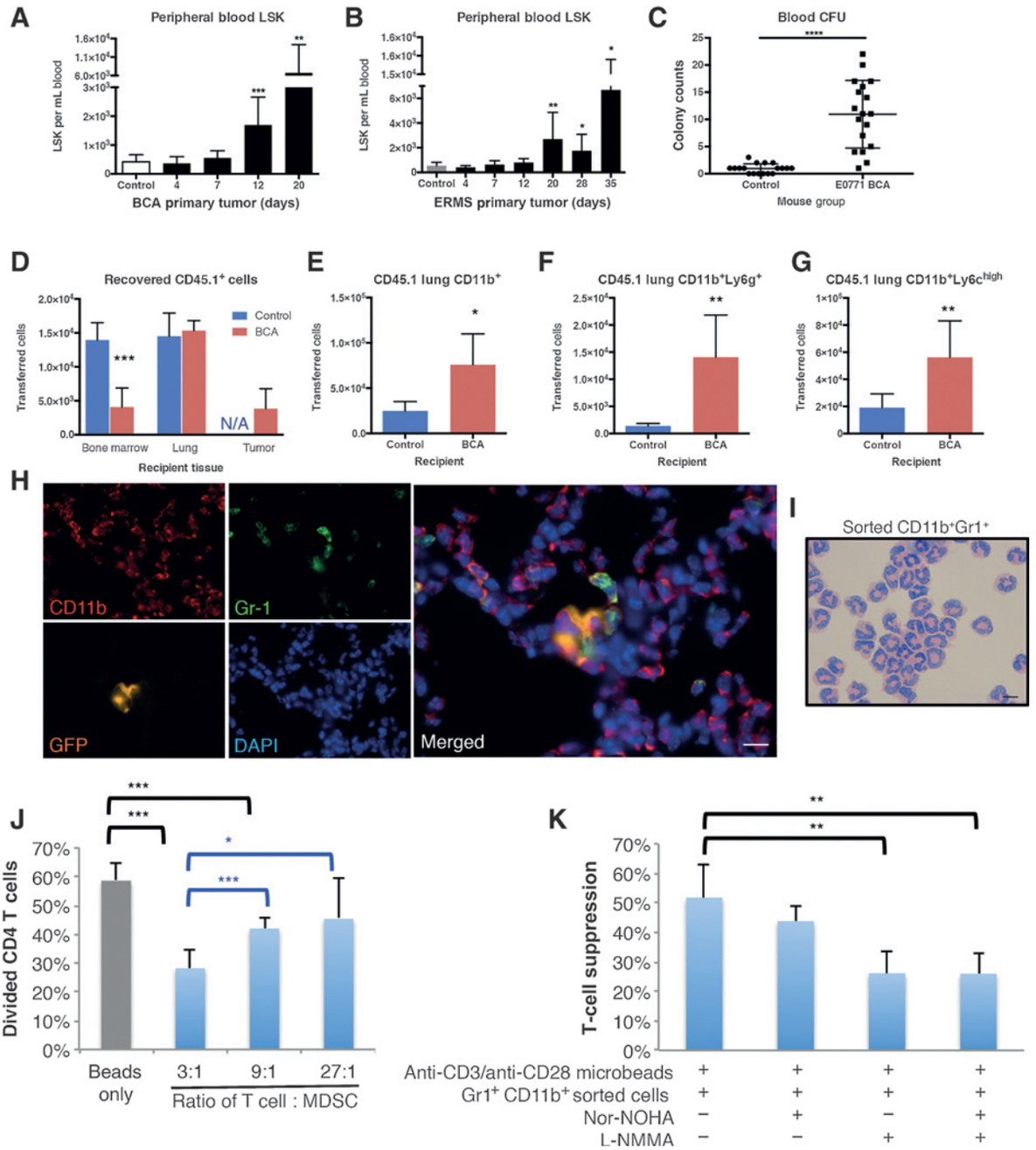

Figure 2.

LSK HSPCs are mobilized and develop into immunosuppressive myeloid cells in tumor-bearing mice. A, LSK cells per milliliters of total live RBC-lysed blood from HBSS control or E0771 tumor-bearing mice ($n = 12$ for control mice; $n = 4$ for each tumor-bearing mouse group). B, LSK cells per milliliters of total live RBC-lysed blood in HBSS control or M3-9-M tumor-bearing mice ($n = 6$ mice per group). C, CFU colony counts of circulating blood from mice without tumor or bearing E0771 tumor for 12 days ($n = 6$ mice per group; blood from each mouse plated in duplicate). D–G, flow cytometry–sorted LSK cells from bone marrow of E0771 BCA tumor-bearing CD45.1 donor mice were intravenously injected into either control or E0771 BCA tumor-bearing CD45.2 recipients. Tissues were harvested 24 hours after injection of LSK cells and analyzed by flow cytometry. D, number of CD45.1$^+$ donor cells detected in the indicated tissues of control or E0771 BCA tumor-bearing recipients ($n = 5$ mice per group). E–G, flow cytometry analysis of CD45.1$^+$ donor-derived cells in lungs of control or premetastatic E0771 BCA tumor-bearing recipient mice to quantify CD11b$^+$ cells (B), CD11b$^+$Ly6g$^+$ cells (C), and CD11b$^+$Ly6c^{hi} cells (D) that differentiated from transferred LSK cells ($n = 5$ mice per group). H, immunofluorescence of lungs stained with the indicated antibodies (CD11b, Gr-1, GFP) and DAPI and imaged under ×63 magnification. Scale bar, 10 μm. I, Diff-Quik staining of cytospins from flow cytometry sorted CD11b$^+$Gr-1$^+$ cells from IVIS-negative E0771 ffluc-GFP tumor-bearing mice. Scale bar, 10 μm. J, T cells were incubated with the indicated ratio of CD11b$^+$Gr-1$^+$ cells isolated from IVIS-negative lungs of E0771 ffluc-GFP tumor-bearing mice and stimulated with anti-CD3/anti-CD28 microbeads. T-cell division was assessed by Cell Trace Violet dilution after 4 days. Error bars, SD for each group ($n = 5$ replicates). K, anti-CD3/anti-CD28-stimulated T cells were incubated with CD11b$^+$Gr-1$^+$ cells at a 3:1 ratio with the indicated small-molecule inhibitors. T-cell proliferation was assessed as in H. Each sample represents $n = 5$ replicates, nor-NOHA (arginase inhibitor), L-NMMA (iNOS inhibitor). Percent suppression is relative to T cells incubated with anti-CD3/anti-CD28 microbeads only. *, $P < 0.05$; **, $P < 0.005$; ***, $P < 0.005$; ****, $P < 0.0001$.

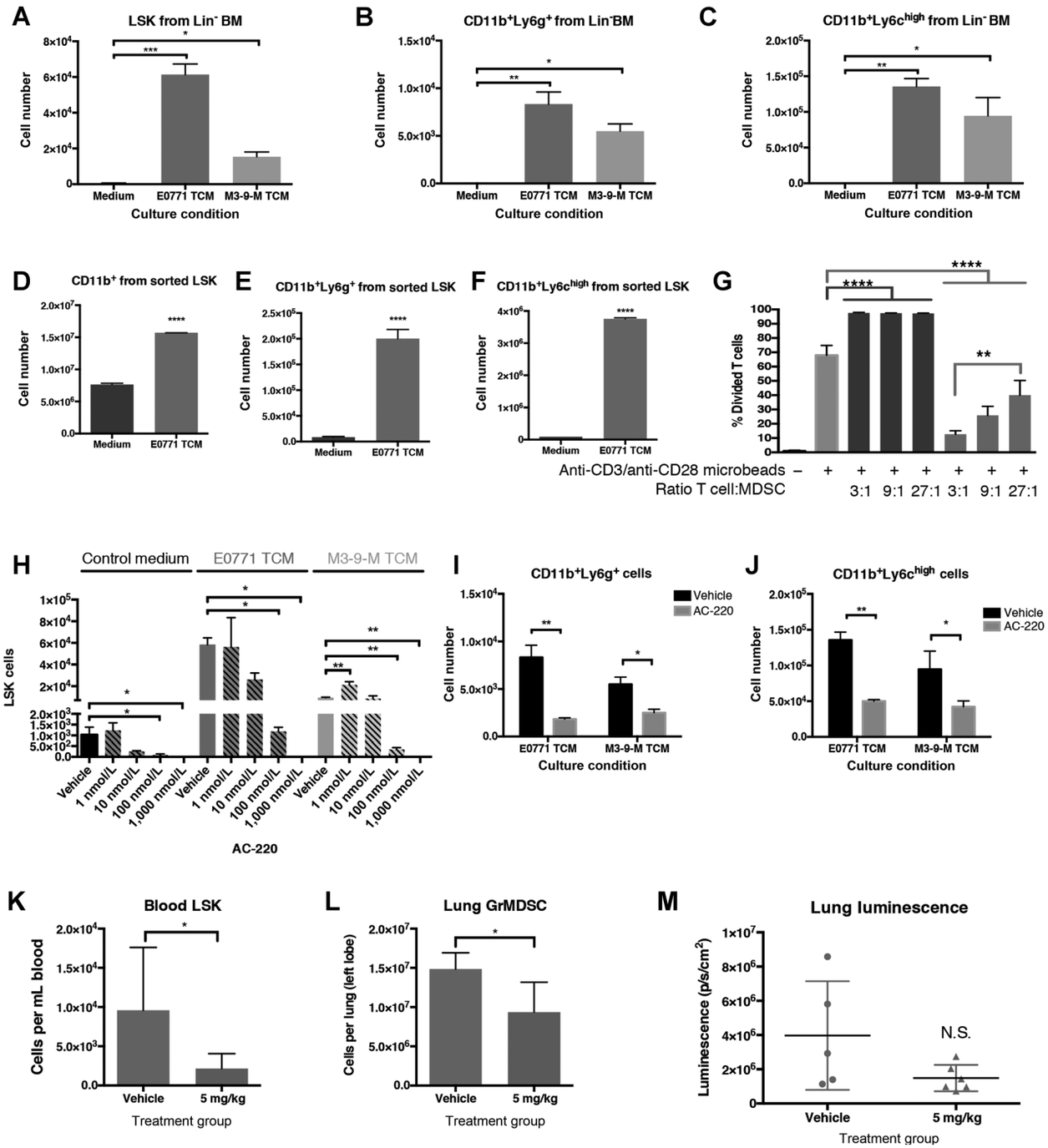

Figure 3.

Tumor-derived factors expand LSK and promote myeloid development. A–C, flow cytometry analysis of lineage-depleted bone marrow (BM) cells after 7 days of culture with control medium or medium conditioned by E0771 BCA (E0771 TCM) or M3-9-M ERMS (M3-9-M TCM). LSK (Lineage$^-$Sca1$^+$CD117$^+$), GrMDSC (CD11b$^+$Ly6g$^+$), and MoMDSC (CD11b$^+$Ly6c^{hi}) were quantified. $n = 2$ wells per condition. D–F, flow cytometry-sorted LSK cells were cultured with control medium or E0771 BCA tumor-conditioned medium (E0771 TCM). The number of CD11b$^+$ (D), CD11b$^+$Ly6g$^+$ (E), or CD11b$^+$Ly6c^{hi} (F) produced in culture were quantified by flow cytometry. $n = 3$ wells per condition. G, cultured cells from sorted LSK in (D–F) were incubated at the indicated ratio with anti-CD3/anti-CD28-stimulated T cells. T-cell division was assessed by CellTrace Violet dilution of CD3$^+$ cells. $n = 3$ wells per condition. H, lineage-depleted bone marrow was cultured with control medium, E0771 BCA TCM, or M3-9-M ERMS TCM for 7 days. Vehicle or the FLT3 inhibitor AC-220 was added at the indicated concentration. LSK cells were quantified by flow cytometry analysis. $n = 2$ wells per condition. I–J, lineage-depleted bone marrow was cultured with E0771 BCA TCM or M3-9-M ERMS TCM for 7 days with vehicle or 100 nmol/L AC-220. CD11b$^+$Ly6g$^+$ (I) and CD11b$^+$Ly6c^{high} cells (J) were quantified by flow cytometry analysis. $n = 2$ wells per condition. K and L, mice-bearing E0771 BCA primary tumors were treated daily with vehicle or AC-220. Mice were euthanized on treatment day 8. LSK cells were quantified in circulating blood (K), and CD11b$^+$Ly6g$^+$ cells were quantified in lung (L). M, luminescence of dissected lungs from mice in K and L. $n = 5$ (control) and 7 (5 mg/kg) mice per group. *, $P < 0.05$; **, $P < 0.005$; ***, $P < 0.005$; ****, $P < 0.0001$. N.S., nonsignificant.

FLT3 ligand synergistically expanded LSK HSPCs cultured in E0771 BCA TCM and M3-9-M ERMS TCM (Supplementary Fig. S6E). Therefore, FLT3 was targeted as a common pathway for tumor-mediated stem cell expansion. AC-220, a second-generation FLT3 receptor inhibitor, effectively blocked LSK expansion in control medium at 100 nmol/L, reflecting the ability of this inhibitor to block the FLT3 ligand supplemented in this culture system (Fig. 3H). LSK expansion mediated by E0771 BCA and M3-9-M ERMS TCM was reduced by over 90% with 100 nmol/L AC-220 relative to vehicle. Furthermore, FLT3 blockade significantly inhibited both $CD11b^{+}Ly6g^{+}$ and $CD11b^{+}Ly6c^{high}$ myeloid cell production from TCM (Fig. 3I and J).

We next sought to determine whether targeting FLT3 ligand could diminish tumor-mediated LSK expansion *in vivo*. Mice bearing 0.5 cm E0771 BCA primary tumors were treated daily with vehicle or 5 mg/kg AC-220 for 8 days. Mice treated with AC-220 had diminished levels of circulating LSK HSPCs relative to vehicle-treated mice (Fig. 3K). Furthermore, $CD11b^{+}Ly6g^{+}$ myeloid cells were decreased in lungs of AC-220–treated tumor-bearing mice relative to vehicle-treated tumor-bearing mice (Fig. 3L). These data were accompanied by a notable decrease in tumor-derived luminescence in the lungs of AC-220–treated mice (Fig. 3M). Together, these data suggest that tumor-derived factors promote LSK HSPC expansion and differentiation into immunosuppressive myeloid subsets. By targeting tumor-mediated HSPC expansion through FLT3 inhibition, both LSK HSPC mobilization and $CD11b^{+}Ly6g^{+}$ accumulation at early metastatic sites are diminished.

Circulating HSPCs promote experimental metastasis

We next sought to determine whether mobilization of HSPCs could confer a survival advantage to disseminating tumor cells. To mimic the surge in circulating LSK HSPCs induced by a primary tumor, we targeted the CXCL12 pathway that tethers LSK within the bone marrow niche. This pathway was targeted due to our earlier finding that the CXCL12:CXCR4 axis was altered in the bone marrow of tumor-bearing mice (Supplementary Fig. S2A). We utilized the CXCR4 receptor antagonist AMD3100, which rapidly and acutely mobilizes CXCR4-expressing hematopoietic cells by transiently blocking the CXCR4:CXCL12 axis when administered in a single dose (30, 31). Importantly, AMD3100, similar to G-CSF, mobilizes HSPCs but does not promote myeloid lineage skewing as seen with G-CSF.

A single dose of AMD3100 elevated circulating LSK HSPCs to over twice basal levels within 1 hour of treatment (Fig. 4A). Mice that first received one dose of AMD3100 followed by tail-vein injection of E0771 BCA tumor cells developed more metastases and had a significantly shorter survival time than control mice that were given PBS prior to tail-vein injection (median survival of 28 days for AMD3100 vs. 48 days for PBS; Fig. 4B and C). Thus, short-term mobilization of hematopoietic cells directly influences metastatic survival. Evaluation of the lungs at 2 weeks posttumor injection revealed significantly greater numbers of $CD11b^{+}Ly6g^{+}$ granulocytic MDSCs in the lungs of PBS-treated tumor-bearing mice and AMD3100-treated tumor-bearing mice relative to non-tumor-bearing control mice (Fig. 4D and E). However, within tumor-bearing subsets, those mice pretreated with AMD3100 contained significantly greater numbers of granulocytic MDSCs relative to mice pretreated with PBS. Thus, mobilization of LSK HPSCs resulted in increased $CD11b^{+}Ly6g^{+}$ cells in metastatic sites and an overall increase in metastatic progression. Prior to injection, E0771 BCA cells were assessed for CXCR4 receptor expression by flow cytometry, and it was found to be absent, indicating that AMD3100 was working through a direct effect on HSPC mobilization (Supplementary Fig. S2E).

As we determined that circulating HSPCs differentiated into myeloid cells in the premetastatic site, we hypothesized that immune evasion may provide one mechanism by which HSPCs promoted metastasis. Loss of radiosensitive hematopoietic cells completely abrogated the metastasis-promoting effects of AMD3100 pretreatment, further implicating this population in metastatic progression (Fig. 5A). In addition, mobilization of LSK HSPCs by AMD3100 had no effect on metastatic burden or survival in immunodeficient SCID/Beige mice, demonstrating that the enhanced metastatic effect of AMD3100 is not tumor-intrinsic but due to T-cell–dependent immunosuppression (Fig. 5B). Finally, to specifically assess the functional role of LSK HSPC differentiation into myeloid cells during metastatic progression, we utilized a monoclonal anti-Gr-1 antibody to specifically target Gr-1–expressing myeloid cells. The metastasis-promoting effect of AMD3100 treatment was completely abrogated with anti-Gr-1 treatment (Fig. 5C–F). Together, these data suggest a model whereby mobilized LSK HSPCs provide an upstream component to the immunosuppressive microenvironment and contribute to immunosuppressive myeloid populations within pre/early metastatic sites.

Mobilized HSPCs as a marker of metastatic progression

We next sought to determine whether mobilized HSPCs observed in our murine models could translate to clinical samples. Consistent with our murine studies, blood from patients with rhabdomyosarcoma or early-stage breast cancer displayed significantly enhanced granulocytic/monocytic CFU potential, demonstrating that circulating HSPCs were present in patients with cancer (Fig. 6A and B). We further sought to evaluate whether the level of circulating HSPCs marked by VEGFR1 and CD34, an established marker for human HSPCs, were associated with risk of metastatic disease in patients with cancer. In rhabdomyosarcoma patients stratified by standard risk assessment, those patients with the highest risk of metastasis had the highest levels of circulating $VEGFR1^{+}CD34^{+}$ HSPCs (Fig. 6C). We also examined blood from 75 breast carcinoma patients with early-stage disease for circulating VEGFR1-expressing HSPCs. In breast carcinoma, there is growing support for stratification of patients based on molecular subtype, and these subtypes show differential risk of metastatic disease, disease recurrence, and clinical outcome and risk for death due to disease (32). Patients with all subtypes of invasive breast carcinoma had increased circulating HSPCs at diagnosis relative to patients with nonmetastatic, noninvasive ductal carcinoma *in situ* (DCIS; Fig. 6D). These findings are supported by recent work in xenograft breast cancer dormancy models (9). Intriguingly, the highest level of circulating HSPCs relative to DCIS and those patients with luminal A subtype were seen in patients with the triple-negative molecular subtype, which is associated with a higher risk for disease progression ($P < 0.005$).

To determine whether circulating HSPCs could predict metastatic relapse, we prospectively measured circulating HSPC levels in newly diagnosed rhabdomyosarcoma patients. The patients who proceeded to develop metastatic progression had significantly greater levels of circulating HSPCs at time of diagnosis than

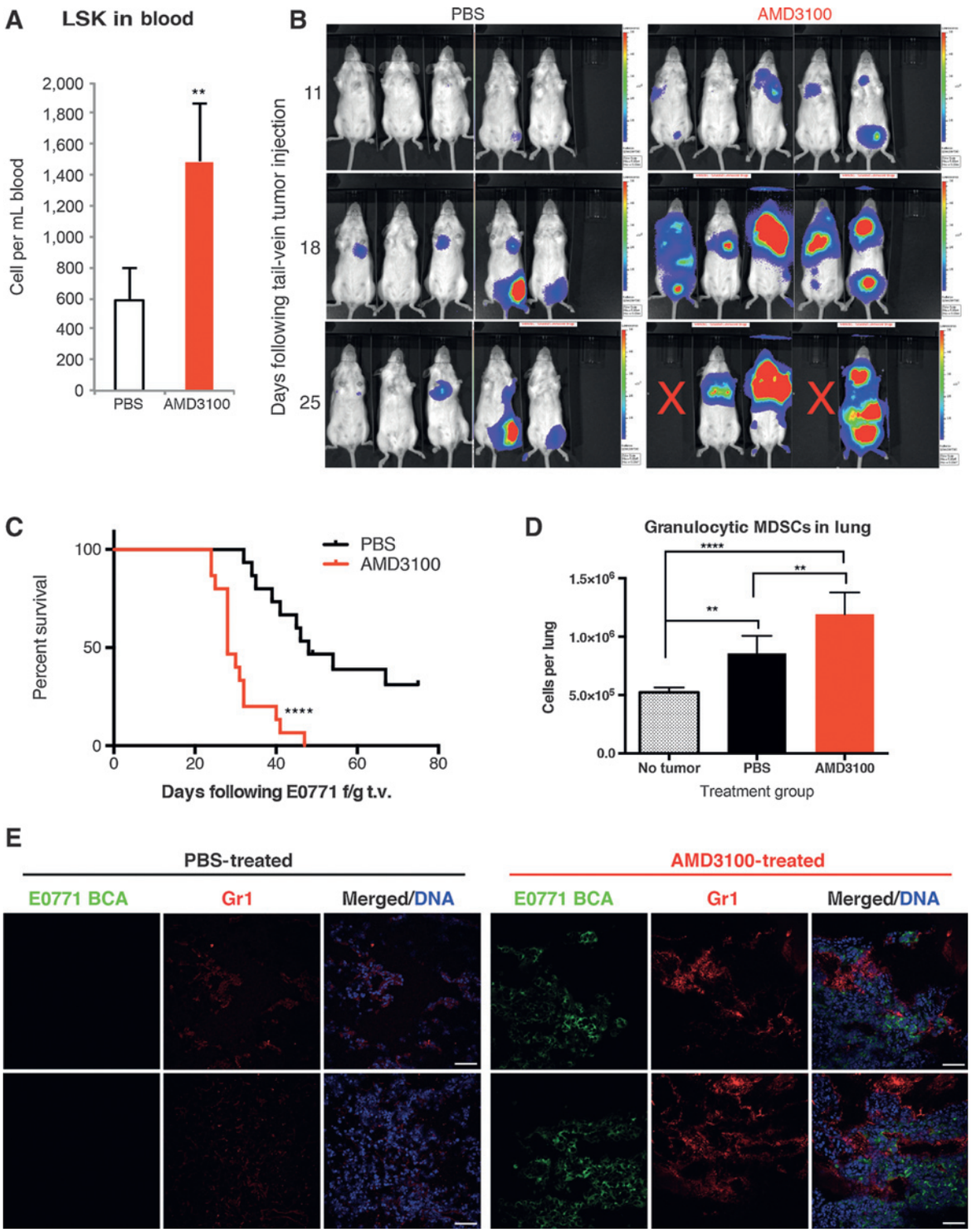

Figure 4.

Mobilization of LSK cells by AMD3100 enhances experimental metastasis. A, mice were injected with PBS or AMD3100 and blood samples taken 1 hour after injection. Circulating LSK HSPCs were quantified by flow cytometry ($n = 5$ mice per group). B, mice were injected with PBS (Control) or AMD3100. One hour after treatment, E0771 ffluc-eGFP tumor cells were injected via tail vein. IVIS images were acquired at the indicated times following tail-vein injection of tumor cells. C, survival of mice pretreated with PBS or AMD3100 followed by tail-vein injection of E0771-ffluc-GFP tumor cells as in B (data are combined from three independent experiments of $n = 5$ mice per group). D, flow cytometry analysis of $CD11b^{+}Ly6g^{+}$ cells in lungs from mice that received no tail-vein tumor or E0771 ffluc-eGFP tail-vein tumor 1 hour following treatment as in B and C. Lungs were analyzed 14 days following tumor injection ($n = 5$ mice per group). E, representative immunofluorescence of lungs from mice in the indicated treatment group and tail-vein injected with E0771 ffluc-eGFP. Lung sections were stained with the indicated antibodies (GFP for tumor, Gr1) and DRAQ5 for nuclear detection. Images acquired with ×40 magnification. Scale bar, 50 μm. **, $P < 0.005$; ****, $P < 0.0001$.

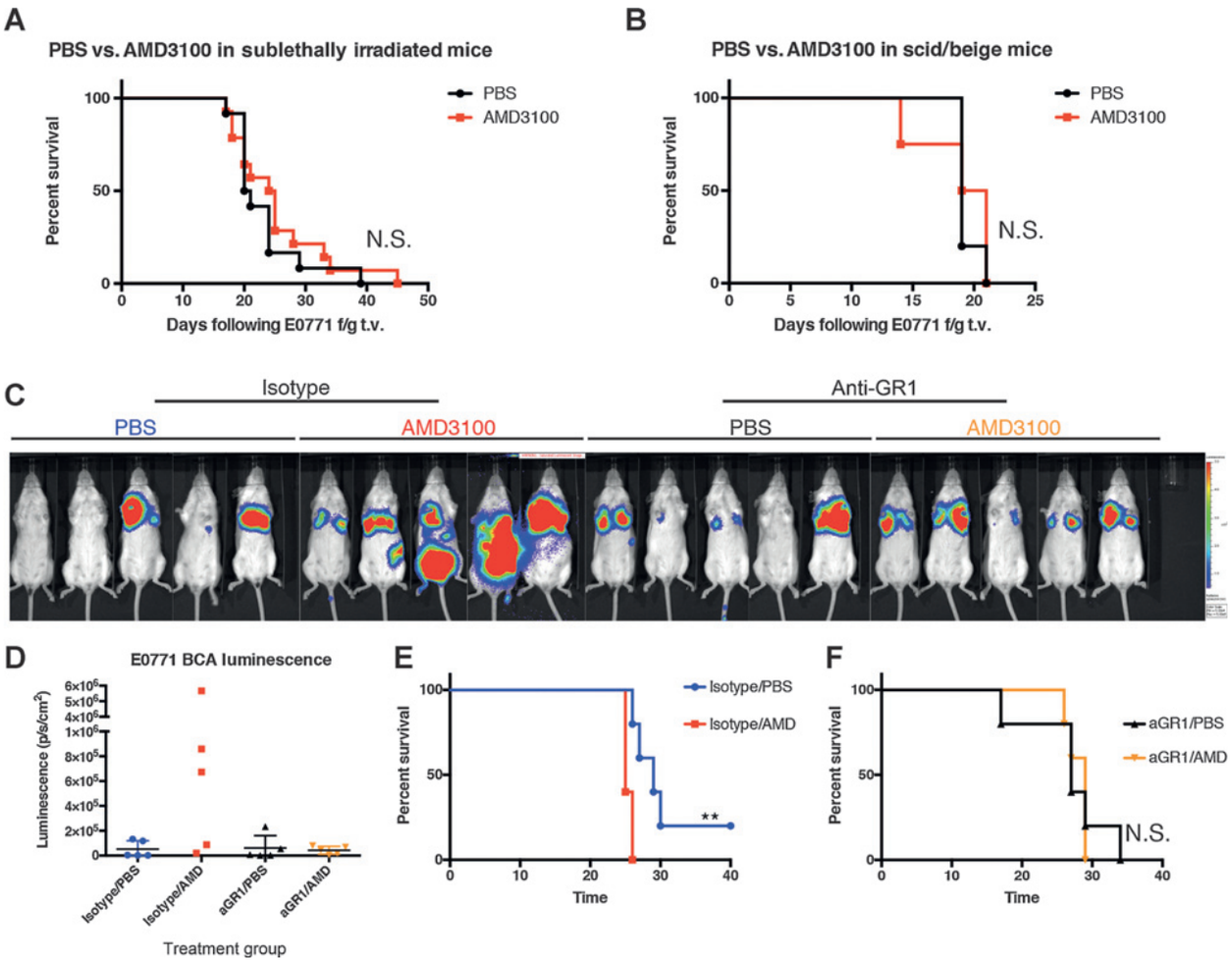

Figure 5.
Promotion of experimental metastasis by AMD3100 requires an intact immune system. A, survival of mice that had received sublethal irradiation prior to treatment with PBS or AMD3100. One hour after PBS or AMD3100 treatment, mice received tail-vein injection of E0771 ffluc-GFP tumor ($n = 5$ mice per group). B, survival of SCID/beige mice treated with PBS or AMD3100 followed by tail-vein injection of E0771 ffluc-GFP tumor 1 hour following treatment ($n = 5$ mice per group). C, luminescence images of mice that were administered anti-Gr-1 antibody or isotype antibody 24 hours before treatment with PBS or AMD3100. E0771ffluc-eGFP tumor cells were administered by tail-vein injection 1 hour following PBS or AMD3100 treatment. IVIS images were taken two weeks following injection of tumor. D, quantification of total body luminescence from mice in C. E and F, survival of mice administered isotype antibody followed by AMD3100 or PBS (E) and mice administered anti-Gr-1 antibody followed by AMD3100 or PBS (F). **, $P < 0.005$. N.S., nonsignificant.

patients who did not relapse. This suggests that this marker, if validated in larger cohorts, could predict at the time of diagnosis which patients are most likely to develop relapsed metastatic disease, even within an intermediate or high-risk subpopulation (Fig. 6E). Together, these data suggest that circulating HSPCs in both murine models and cancer patients can contribute to the metastatic process and may be used to identify populations at great risk for metastatic relapse.

Discussion

The bone marrow responds to cues from distant tissues during stresses such as infection, inflammation, and wound healing and induces hematopoietic stem cells to reversibly exit quiescence, expand, and enter circulation (33–35). During a wound-healing response, local tissue production of chemoattractants, toll-like receptor ligands, and integrins can attract and bind circulating HSPCs (36). Although many parallels have been made between inflammation and cancer, we and others are beginning to shed light upon the essential role of the bone marrow microenvironment that supports hematopoiesis during cancer metastasis (9, 37–40).

LSK HPSCs were elevated in both the bone marrow and blood of E0771 BCA and M3-9-M ERMS tumor-bearing mice at pre-/early metastatic times. LSK HSPCs in the bone marrow were actively expanding as assessed by BrdUrd incorporation. Short-term HSCs and multipotent progenitors contributed to the expansion of LSK HSPCs, yet long-term HSC numbers remained unchanged until the last day of tumor growth, at which time mice were euthanized due to primary tumor size. This pattern of progenitor expansion permits a hematopoietic response to a primary tumor while maintaining the long-term stem cell pools, and thus preventing hematopoietic exhaustion.

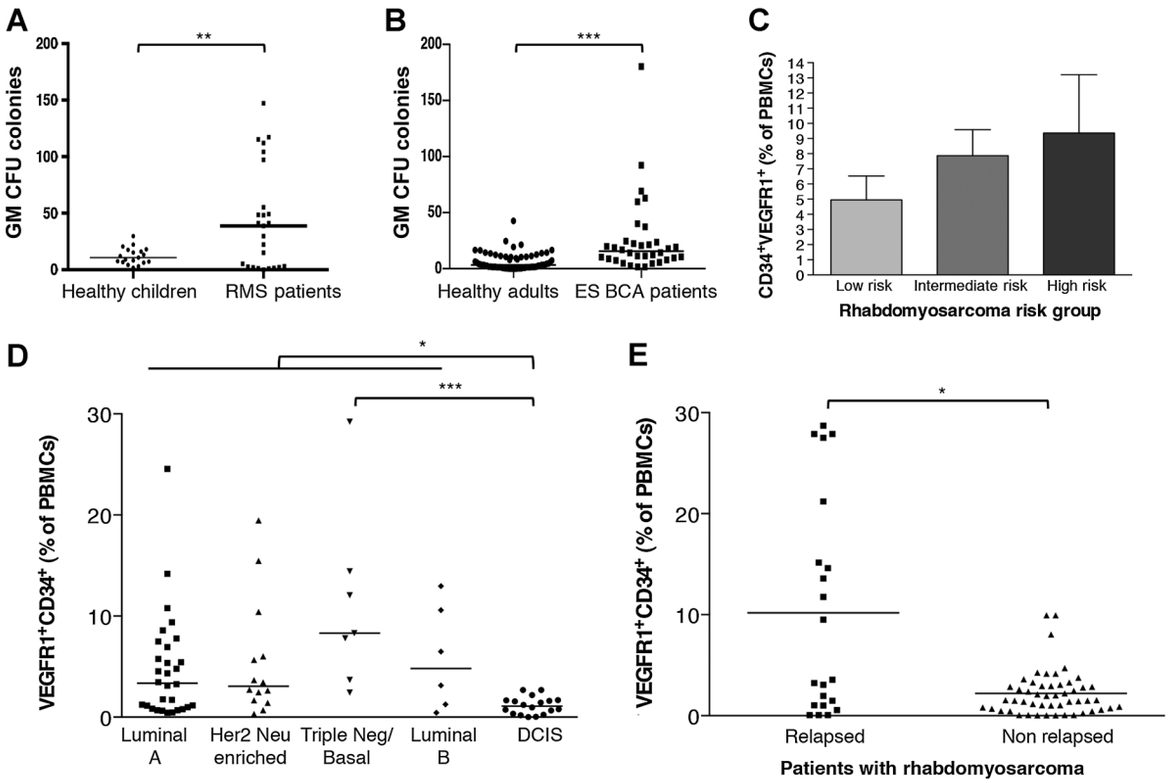

Figure 6.

Elevated circulating progenitor cells in patients with cancer predict metastatic risk. A, GM CFUs per 100,000 PBMCs from blood of healthy control children ($n = 19$) or patients with rhabdomyosarcoma ($n = 25$) at time of diagnosis. B, GM CFUs per 100,000 PBMNCs of healthy control adults ($n = 68$) or patients with early-stage breast cancer at time of diagnosis (ES BCA, $n = 34$). C, flow cytometry analysis of circulating $VEGFR1^+CD34^+$ progenitor cells analyzed at time of diagnosis correlate with metastatic risk of rhabdomyosarcoma patients ($n = 5$ for low risk; $n = 20$ for intermediate risk; $n = 25$ for high risk). D, circulating $VEGFR1^+CD34^+$ progenitor cells analyzed at time of diagnosis correlate with metastatic risk of patients with early-stage breast cancer [$n = 30$ for luminal A; $n = 14$ for Her2 Neu enriched; $n = 7$ for triple-negative (Triple Neg)/basal; $n = 6$ for Luminal B; $n = 18$ for DCIS]. I, elevated circulating $VEGFR1^+CD34^+$ progenitor cells in rhabdomyosarcoma patients at time of diagnosis predicts metastatic relapse. *, $P < 0.05$; **, $P < 0.005$; ***, $P < 0.005$.

Recent studies have implicated immunosuppressive hematopoietic cells in the premetastatic lung environment (11, 41). Here, we show circulating HSPCs function to promote metastasis by developing into immunosuppressive cells within the premetastatic site. Using *ex vivo* culture, we demonstrated that tumor-derived factors expanded LSK HSPCs and also promoted differentiation of these cells into immunosuppressive myeloid cells. We further showed that purified LSK HSPCs differentiated *in vivo* into immunosuppressive myeloid cells within in a premetastatic site. Although we identified multiple cytokines capable of expanding LSK HSPCs in E0771 BCA and M3-9-M ERMS tumor-conditioned media, including FLT3 ligand, we found that FLT3 inhibition with AC-220 significantly impaired tumor factor–mediated LSK expansion *ex vivo*. FLT3 inhibition in tumor-bearing mice decreased levels of circulating LSK HSPCs and $CD11b^+Ly6g^+$ found in metastatic sites.

We implicate circulating HSPCs as active players in metastatic progression by utilizing the stem cell–mobilizing agent AMD3100. AMD3100 disrupts the CXCR4:CXCL12 interaction that tethers CXCR4-expressing HSPCs in the bone marrow. We found this axis was disrupted in tumor-bearing mice, likely contributing to the increase in circulating stem cells. Mice treated with single-dose AMD3100 demonstrated a significant increase in experimental metastasis and shorter survival relative to PBS-treated mice. This was accompanied by a significant increase in $CD11b^+Ly6g^+$ cells in the lungs of AMD3100 pretreated mice. We further demonstrate that the metastasis-promoting effect of HSPC mobilization is lost in immunodeficient mice and in Gr-1–depleted mice. Importantly, this model utilized a short exposure of AMD3100 to increase HSPC levels in peripheral tissues, as constitutive blockade of the CXCR4:CXCL12 signaling axis results in severe depletion of the hematopoietic stem cell pool, including $Gr1^+$ cells (42). These data are consistent with our *ex vivo* and *in vivo* data that demonstrate purified LSK HSPCs develop into immunosuppressive myeloid cells in response to tumor-derived factors. Furthermore, our data build upon previous studies in which constitutive blockade of the CXCR4:CXCL12 signaling axis results in diminished $Gr1^+$ cell numbers, decreased $Gr1^+$ cell infiltration into distant tissues, and therefore decreased metastasis, in tumor-bearing mice (43). The immunosuppressive microenvironment afforded by these $Gr1^+$ cells likely provides sanctuary to seeding tumor, thus tipping the balance to immune escape and metastatic progression.

We found that HSPCs are elevated in the circulation of cancer patients at time of diagnosis and are particularly elevated in those patients who develop metastatic relapse. Together, these data suggest that circulating HSPCs can serve as a potential dynamic microenvironmental marker that could add an additional dimension to standard tumor assessment in determining metastatic risk.

Larger scale clinical studies are needed to flesh out the utility of this dynamic microenvironmental measurement as a biomarker to predict metastatic risk and response to therapy. This would include parsing out the utility of HSPC mobilization relative to circulating MDSC numbers or inflammatory monocyte precursors relative to tumor-associated macrophages. These approaches could have a tremendous impact in the clinical setting and provide not only one of the earliest prognostic tools for determining metastatic risk but a novel strategy to redirect the altered hematopoiesis and wound healing response that occurs during metastatic progression.

Much focus has been placed on biomarkers stemming from the molecular characteristics of the tumor cells. However, few biomarkers exist in human studies that measure the supportive cells of the premetastatic microenvironment that are crucial to metastatic progression. Here, we find that circulating HSPCs can serve as a window into premetastatic niche formation. HSPCs represent a plastic population at the branch point of hematopoietic development, and thus there is potential to manipulate the differentiation route of these stem cells from a tumor-promoting to a tumor-suppressing phenotype. Studies aimed at uncovering the detailed molecular crosstalk within stem cell niches and determining how external environmental cues from a growing complex of tumor cells, immune cells, and stromal cells induce a chronic injury response in the bone marrow microenvironment will lead to new therapeutic approaches and successful immunotherapy adjuvants to target metastasis.

Disclosure of Potential Conflicts of Interest

No potential conflicts of interest were disclosed.

Authors' Contributions

Conception and design: A.J. Giles, C.M. Reid, J.D.W. Evans, Y. Vicioso, S.L. Highfill, D. Lyden, L. Wexler, R.N. Kaplan

Development of methodology: A.J. Giles, C.M. Reid, J.D.W. Evans, M. Murgai, Y. Vicioso, R.N. Kaplan

Acquisition of data (provided animals, acquired and managed patients, provided facilities, etc.): A.J. Giles, C.M. Reid, M. Murgai, Y. Vicioso, M. Kasai, L. Vahdat, L. Wexler, R.N. Kaplan

Analysis and interpretation of data (e.g., statistical analysis, biostatistics, computational analysis): A.J. Giles, C.M. Reid, J.D.W. Evans, M. Murgai, Y. Vicioso, M. Kasai, C.L. Mackall, D. Lyden, R.N. Kaplan

Writing, review, and/or revision of the manuscript: A.J. Giles, C.M. Reid, J.D.W. Evans, M. Murgai, Y. Vicioso, S.L. Highfill, C.L. Mackall, R.N. Kaplan

Administrative, technical, or material support (i.e., reporting or organizing data, constructing databases): A.J. Giles, J.D.W. Evans, M. Kasai, M. Murgai, R.N. Kaplan

Study supervision: A.J. Giles, L. Wexler, R.N. Kaplan

Acknowledgments

The authors thank K. McKinnon at the Vaccine Branch FACS core (NCI) for help with cell sorting; A. Merchant at the Center for Cancer Research Bioinformatics Core (NCI) for help with microarray analysis; L. Rotman, E. Bomszytk, R.M. Andre, M. R. Domsai, and C. Persenairre for outstanding technical support; P. Steeg, L. Wakefield, R. Germain, and C. Thiele for critical review of the manuscript.

The costs of publication of this article were defrayed in part by the payment of page charges. This article must therefore be hereby marked *advertisement* in accordance with 18 U.S.C. Section 1734 solely to indicate this fact.

Received January 20, 2015; revised October 5, 2015; accepted November 24, 2015; published OnlineFirst December 30, 2015.

References

1. Wan L, Pantel K, Kang Y. Tumor metastasis: moving new biological insights into the clinic. Nat Med 2013;19:1450–64.
2. Joyce JA, Pollard JW. Microenvironmental regulation of metastasis. Nat Rev Cancer 2009;9:239–52.
3. Lander AD, Kimble J, Clevers H, Fuchs E, Montarras D, Buckingham M, et al. What does the concept of the stem cell niche really mean today? BMC Biol 2012;10:19.
4. Bhat R, Bissell MJ. Of plasticity and specificity: dialectics of the microenvironment and macroenvironment and the organ phenotype. Wiley Interdiscip Rev Dev Biol 2014;3:147–63.
5. Littlepage LE, Egeblad M, Werb Z. Coevolution of cancer and stromal cellular responses. Cancer Cell 2005;7:499–500.
6. McAllister SS, Weinberg RA. The tumour-induced systemic environment as a critical regulator of cancer progression and metastasis. Nat Cell Biol 2014;16:717–27.
7. Oskarsson T, Batlle E, Massague J. Metastatic stem cells: sources, niches, and vital pathways. Cell Stem Cell 2014;14:306–21.
8. Kaplan RN, Riba RD, Zacharoulis S, Bramley AH, Vincent L, Costa C, et al. VEGFR1-positive haematopoietic bone marrow progenitors initiate the pre-metastatic niche. Nature 2005;438:820–7.
9. McAllister SS, Gifford AM, Greiner AL, Kelleher SP, Saelzler MP, Ince TA, et al. Systemic endocrine instigation of indolent tumor growth requires osteopontin. Cell 2008;133:994–1005.
10. Oskarsson T, Acharyya S, Zhang XH, Vanharanta S, Tavazoie SF, Morris PG, et al. Breast cancer cells produce tenascin C as a metastatic niche component to colonize the lungs. Nat Med 2011;17:867–74.
11. Sceneay J, Chow MT, Chen A, Halse HM, Wong CS, Andrews DM, et al. Primary tumor hypoxia recruits CD11b+/Ly6Cmed/Ly6g+ immune suppressor cells and compromises NK cell cytotoxicity in the premetastatic niche. Cancer Res 2012;72:3906–11.
12. Kim S, Takahashi H, Lin WW, Descargues P, Grivennikov S, Kim Y, et al. Carcinoma-produced factors activate myeloid cells through TLR2 to stimulate metastasis. Nature 2009;457:102–6.
13. Xing F, Okuda H, Watabe M, Kobayashi A, Pai SK, Liu W, et al. Hypoxia-induced Jagged2 promotes breast cancer metastasis and self-renewal of cancer stem-like cells. Oncogene 2011;30:4075–86.
14. Wong CC, Zhang H, Gilkes DM, Chen J, Wei H, Chaturvedi P, et al. Inhibitors of hypoxia-inducible factor 1 block breast cancer metastatic niche formation and lung metastasis. J Mol Med 2012;90:803–15.
15. Hiratsuka S, Watanabe A, Sakurai Y, Akashi-Takamura S, Ishibashi S, Miyake K, et al. The S100A8-serum amyloid A3-TLR4 paracrine cascade establishes a pre-metastatic phase. Nat Cell Biol 2008;10:1349–55.
16. Ogawa F, Amano H, Eshima K, Ito Y, Matsui Y, Hosono K, et al. Prostanoid induces premetastatic niche in regional lymph nodes. J Clin Invest 2014;124:4882–94.
17. Labelle M, Begum S, Hynes RO. Platelets guide the formation of early metastatic niches. Proc Natl Acad Sci U S A 2014;111:E3053–61.
18. Cox TR, Bird D, Baker AM, Barker HE, Ho MW, Lang G, et al. LOX-mediated collagen crosslinking is responsible for fibrosis-enhanced metastasis. Cancer Res 2013;73:1721–32.
19. Erler JT, Bennewith KL, Cox TR, Lang G, Bird D, Koong A, et al. Hypoxia-induced lysyl oxidase is a critical mediator of bone marrow cell recruitment to form the premetastatic niche. Cancer Cell 2009;15:35–44.
20. Liu S, Jiang M, Zhao Q, Li S, Peng Y, Zhang P, et al. Vascular endothelial growth factor plays a critical role in the formation of the pre-metastatic niche via prostaglandin E2. Oncol Rep 2014;32:2477–84.
21. Chambers AF, Groom AC, MacDonald IC. Dissemination and growth of cancer cells in metastatic sites. Nat Rev Cancer 2002;2:563–72.
22. Luzzi KJ, MacDonald IC, Schmidt EE, Kerkvliet N, Morris VL, Chambers AF, et al. Multistep nature of metastatic inefficiency: dormancy of solitary cells after successful extravasation and limited survival of early micrometastases. Am J Pathol 1998;153:865–73.
23. Orford KW, Scadden DT. Deconstructing stem cell self-renewal: genetic insights into cell-cycle regulation. Nat Rev Genet 2008;9:115–28.

24. Wilson A, Laurenti E, Oser G, van der Wath RC, Blanco-Bose W, Jaworski M, et al. Hematopoietic stem cells reversibly switch from dormancy to self-renewal during homeostasis and repair. Cell 2008;135:1118–29.
25. Gabrilovich DI, Ostrand-Rosenberg S, Bronte V. Coordinated regulation of myeloid cells by tumours. Nat Rev Immunol 2012;12:253–68.
26. Youn JI, Nagaraj S, Collazo M, Gabrilovich DI. Subsets of myeloid-derived suppressor cells in tumor-bearing mice. J Immunol 2008;181:5791–802.
27. Highfill SL, Cui Y, Giles AJ, Smith JP, Zhang H, Morse E, et al. Disruption of CXCR2-mediated MDSC tumor trafficking enhances anti-PD1 efficacy. Sci Transl Med 2014;6:237ra67.
28. Lu T, Gabrilovich DI. Molecular pathways: tumor-infiltrating myeloid cells and reactive oxygen species in regulation of tumor microenvironment. Clin Cancer Res 2012;18:4877–82.
29. Heike T, Nakahata T. Ex vivo expansion of hematopoietic stem cells by cytokines. Biochim Biophys Acta 2002;1592:313–21.
30. Liles WC, Broxmeyer HE, Rodger E, Wood B, Hubel K, Cooper S, et al. Mobilization of hematopoietic progenitor cells in healthy volunteers by AMD3100, a CXCR4 antagonist. Blood 2003;102:2728–30.
31. Broxmeyer HE, Orschell CM, Clapp DW, Hangoc G, Cooper S, Plett PA, et al. Rapid mobilization of murine and human hematopoietic stem and progenitor cells with AMD3100, a CXCR4 antagonist. J Exp Med 2005; 201:1307–18.
32. Schnitt SJ. Classification and prognosis of invasive breast cancer: from morphology to molecular taxonomy. Mod Pathol 2010;23 Suppl 2: S60–S4.
33. Lapidot T, Petit I. Current understanding of stem cell mobilization: the roles of chemokines, proteolytic enzymes, adhesion molecules, cytokines, and stromal cells. Exp Hematol 2002;30:973–81.
34. Schuettpelz LG, Link DC. Regulation of hematopoietic stem cell activity by inflammation. Front Immunol 2013;4:204.
35. Sio A, Chehal MK, Tsai K, Fan X, Roberts ME, Nelson BH, et al. Dysregulated hematopoiesis caused by mammary cancer is associated with epigenetic changes and hox gene expression in hematopoietic cells. Cancer Res 2013;73:5892–904.
36. Ziadloo A, Burks SR, Gold EM, Lewis BK, Chaudhry A, Merino MJ, et al. Enhanced homing permeability and retention of bone marrow stromal cells by noninvasive pulsed focused ultrasound. Stem Cells 2012;30: 1216–27.
37. Sethi N, Kang Y. Dysregulation of developmental pathways in bone metastasis. Bone 2011;48:16–22.
38. Trinchieri G. Cancer and inflammation: an old intuition with rapidly evolving new concepts. Annu Rev Immunol 2012;30:677–706.
39. Lu X, Kang Y. Chemokine (C-C motif) ligand 2 engages CCR2+ stromal cells of monocytic origin to promote breast cancer metastasis to lung and bone. J Biol Chem 2009;284:29087–96.
40. Shiozawa Y, Pedersen EA, Havens AM, Jung Y, Mishra A, Joseph J, et al. Human prostate cancer metastases target the hematopoietic stem cell niche to establish footholds in mouse bone marrow. J Clin Invest 2011;121: 1298–312.
41. Yan HH, Pickup M, Pang Y, Gorska AE, Li Z, Chytil A, et al. Gr-1+CD11b+ myeloid cells tip the balance of immune protection to tumor promotion in the premetastatic lung. Cancer Res 2010;70:6139–49.
42. Sugiyama T, Kohara H, Noda M, Nagasawa T. Maintenance of the hematopoietic stem cell pool by CXCL12-CXCR4 chemokine signaling in bone marrow stromal cell niches. Immunity 2006;25:977–88.
43. Hiratsuka S, Duda DG, Huang Y, Goel S, Sugiyama T, Nagasawa T, et al. C-X-C receptor type 4 promotes metastasis by activating p38 mitogen-activated protein kinase in myeloid differentiation antigen (Gr-1)-positive cells. Proc Natl Acad Sci U S A 2011;108: 302–7.